MAGNETIC RESONANCE IN CHEMISTRY, VOL. 35, S37–S46 (1997)

NMR Microscopy and the Non-linear Rheology of Food Materials

Melanie M. Britton and Paul T. Callaghan*
Department of Physics, Massey University, Palmerston North, New Zealand

The non-linear viscosities of a number of different food products were examined using NMR microscopy. These materials included xanthan gum–water solutions, cream, semi-soft butter, egg white, cornflour–water mixtures and two different varieties of tomato sauce. The non-linear rheology is manifest in the velocity profiles measured across pipe, cylindrical Couette cell and cone-and-plate geometries. The properties observed included apparent slip, shear thinning, shear thickening, shear banding and yield stress behaviour. The results show that accurate, non-invasive velocity profiling is essential if the results of mechanical rheometric measurements are to be interpreted correctly. They also illustrate the power of NMR both to demonstrate the existence of and, potentially, to investigate the particulate or molecular origins of complex rheological properties in food materials. © **1997 John Wiley & Sons, Ltd.**

Magn. Reson. Chem. **35**, S37–S46 (1997) No. of Figures: 12 No. of Tables: 0 No. of References: 21

Keywords: NMR; NMR microscopy; viscosity; rheology; food product

Received 23 April 1997; revised 15 July 1997; accepted 15 July 1997

INTRODUCTION

Food materials encompass a diversity of complex fluids. They include polymeric structures, emulsions, particulate solid suspensions, gels and self-assembled micellar lipid phases. It is a defining characteristic of complex fluids that there exists, in the underlying dynamics, a very wide spectrum of intrinsic time-scales and, in particular, time-scales which involve behaviour sufficiently slow to be regarded as 'macroscopic.' The term macroscopic is used here to describe dynamics whose characteristic time (or frequency) is directly detectable in the mechanical properties. A second defining characteristic of complex fluids is that their mechanical properties exhibit both solid- and liquid-like aspects, that is, when subjected to shear, they exhibit not only a viscous response associated with energy dissipation but also an elastic response associated with energy storage. Such behaviour underpins the categorization of a complex fluid in terms of its rheology, a class of analysis in which a fluid is subjected to a wide variety of mechanical measurements. The slow dynamics which are manifest in the mechanical properties include the dynamic (i.e. frequency-dependent) linear viscoelasticity, the stress or strain step response and the shear rate-dependent non-linear viscoelastic behaviour.

The rheological properties of food materials are of particular importance to their manufacture, their processing, their texture, their storage characteristics and their response to changes in temperature and humidity. Rheological science is of fundamental significance to the international food industry. All foods face a mechanical test of over-riding significance during the process of eating. However, at a more fundamental level a wide variety of test procedures are used in industry, ranging from the simplest possible, e.g. the rate of spreading of a food product when laid on a flat surface, to the most sophisticated analyses using apparatus which probes a wide variety of intrinsic mechanical properties. It is with this latter end of the sophistication spectrum with which we shall be concerned in this paper. We shall focus our attention on the measurement of just one particular rheological property, namely the non-linear (i.e. shear-dependent) viscosity and show that the method of NMR velocimetry, which we shall describe here, can provide fresh, and indeed intriguing, insights. In particular, we shall demonstrate that it is possible to obtain velocity images at high spatial resolution using NMR microscopic methods, and that these may reveal localized phase separation within the flow. In consequence, any technique which relies on integral measurement, such as mechanical rheometry, may be in error. Hence NMR can provide new and vital rheological insights. In addition, we note that NMR microscopy is possible with small food samples, of < 1 g. It also allows us to use a standard vertical bore superconducting magnet, the same system as is used for most other applications of NMR in food science.

It could be argued that measurements of non-linear viscosity, although routine in the polymer industry, represent a sophisticated tool in food science. Why, then, should an even more sophisticated and expensive technology, such as NMR, be of interest? As the companion papers in this issue testify, NMR has a host of uses in

* *Correspondence to*: P. T. Callaghan.
Contract grant sponsor: New Zealand Foundation for Research Science and Technology.

© 1997 John Wiley & Sons, Ltd. CCC 0749–1581/97/SI0037–10 $17.50

food technology quite apart from any potential application in mechanical studies and its role is already widely appreciated by food scientists and technologists. Hence, any extension of the application of NMR methods to food studies builds upon an already established base of acceptance within the food industry and implies a greater diversity of use. It is the synergy of the different NMR methods which makes the extension to encompass any new parameter of interest so potentially valuable.

NON-LINEAR RHEOLOGY

When a fluid is subjected to a steady shear it deforms continuously so that the resulting strain (i.e. deformation) increases without limit. In this sense, the fluid is subjected to a non-linear regime of behaviour. This stands in contrast to the case of linear behaviour which occurs when a fluid is subjected to an oscillatory shear in which the resulting strain is kept within strict limits. In the non-linear case the response of the fluid to the stress can be characterized in terms of the steady-state rate of strain established within the fluid. This is illustrated in Fig. 1(a) for the case of parallel plate Couette flow where the rate of strain (i.e. shear rate) is simply $\dot{\gamma} = \partial v_x/\partial y$, the velocity gradient across the gap. For an ideal (Newtonian) fluid, the relationship between stress and strain rate is linear and defines the fluid viscosity, as shown in Fig. 1(b).

The non-linear viscous response of complex fluids may exhibit a wide variety of deviant (i.e. non-Newtonian) behaviour. It is beyond the scope of this paper to review these or the many other aspects of linear- and non-linear rheology which may be of interest in food science. The reader can find such topics fully described in a variety of texts.[1–4] However, we shall find it helpful to focus on just a few examples of importance to food products, which are illustrated in Fig. 2(a) and (b).

The first aspect, shown in Fig. 2(a), is apparent slip. This results from a boundary layer of fluid sustaining a much higher shear rate than the bulk of the fluid, so that there exists an almost discontinuous jump in the fluid velocity near the solid surface through which the stress is applied. Such behaviour generally results from a modification of fluid properties due to the proximity of the solid surface and is therefore dependent on the subtleties of the fluid–solid interaction and, hence the precise nature of each material. Apparent slip is important for two reasons. First, any measurement of viscosity by means of a determination of stress *vs.* rate of strain using a fluid contained between shearing surfaces will usually depend on an assumption that the velocity gradient within the fluid is given simply by the absolute external velocity gradient across the gap between the walls. Where slip occurs this assumption fails completely. Second, apparent slip will generally depend in a subtle and highly non-linear manner on wall stress, and the flow response of the fluid will be largely determined by that relationship. Hence, when considering, for example, at what rate a given fluid may be transferred within a pipe under a given pressure gradient, it may be the apparent slip behaviour rather than the bulk fluidic viscosity which is the principal determinant. In consequence, any flow visualization method which can distinguish apparent slip and bulk shear rate will be of considerable value in elucidating such effects.

The second aspect of non-linear rheology which we shall consider concerns non-Newtonian bulk constitutive properties of the fluid, as distinct from any wall-related phenomena. Several examples of these are illustrated in Fig. 2(b), in which the non-linear viscosity is illustrated by a plot of stress, σ, *vs.* rate-of-strain, $\dot{\gamma}$, a plot known as the 'flow curve.' Figure 2(b) illustrates shear thinning, shear thickening and yield stress behaviour. Shear thinning and shear thickening are character-

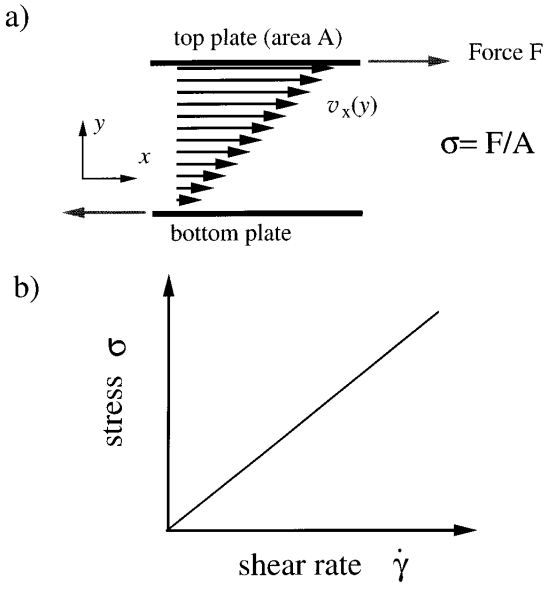

Figure 1. (a) Schematic diagram of parallel plate Couette flow without slip. The shear rate, $\dot{\gamma}$, is $\partial v_x/\partial y$. (b) Flow curve for Newtonian fluids.

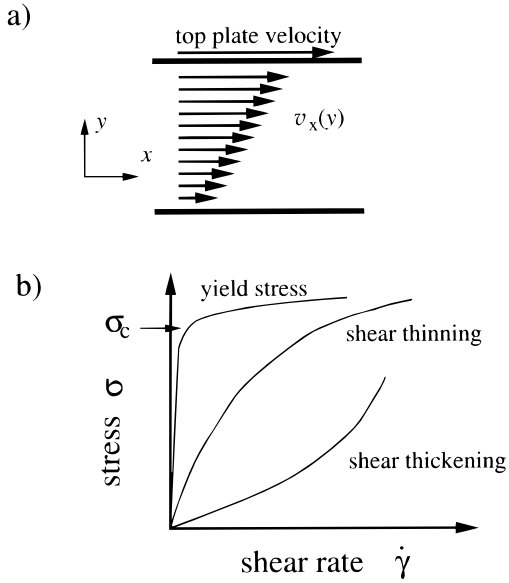

Figure 2. (a) Schematic diagram of parallel plate Couette flow with apparent slip. (b) Flow curves for non-Newtonian fluids.

© 1997 John Wiley & Sons, Ltd.

ized by negative or positive curvature, respectively, in the flow curve and correspond to viscosities decreasing or increasing, respectively, as the rate-of-strain increases. For example, many semi-dilute polymer solutions exhibit shear thinning because the shearing reduces the effect of entanglements[5] or polymer–polymer contacts while some particulate suspensions exhibit shear thickening due to shear-induced aggregation. Xanthan gum solutions and cornflour–water mixtures are examples.

Yield stress behaviour is a form of non-linearity which is particularly apparent in a wide variety of food materials and is manifest by high viscosity at low stress followed by a rapid shear thinning once a critical stress is exceeded. Tomato sauce is a favourite example of such a material. The class of fluids which exhibit critical stress behaviour is of considerable fundamental interest and has been the subject of wide attention by condensed matter theorists in recent years.[6–8] Dramatic examples of model fluids exhibiting yield stress behaviour are provided by the wormlike surfactant systems.[9–11] Above a critical stress these materials exhibit a stress plateau over which the underlying shear rate may be multi-valued. For such a fluid, the velocity profile in the gap between shearing surfaces may be very complex indeed.

SHEARING GEOMETRIES: PIPE FLOW, CYLINDRICAL COUETTE FLOW AND THE CONE-AND-PLATE RHEOMETER

The situation illustrated in Fig. 1(a) is idealised in the extreme. Any practical rheometer used to measure viscosity by means of shearing surfaces will normally be based on continuous rotational motion rather than continuous translational motion. However, the parallel plate Couette geometry in Fig. 1(a) has the particular advantage that the stress within the gap is necessarily uniform as result of the equations of fluid motion and their underlying conservation laws. A very similar situation applies in the rotational cone-and-plate cell shown in Fig. 3(c), provided that the gap angle, α, is kept sufficiently small. The stress across the gap varies as $\mathrm{cosec}^2\,\theta$, where θ is the angle to the polar axis, so that a variation of only 1.5% is sustained with a 7° gap angle. Because the stress is approximately constant across the gap, it is possible to use the cone-and-plate rheometer to step through the flow curve, point by point, obtaining corresponding σ and $\dot{\gamma}$ measurements. Irrespective of whether a fluid is shear-thinning or shear-thickening, and provided that slip effects are absent, the shear rate across the gap should be uniquely defined and identically equal to the rate determined by the external surfaces, $\omega/\tan\alpha$, where ω is the cone rotation speed. In consequence, the cone-and-plate is the pre-eminent device used to study non-linear viscosity in complex fluids. In the present paper we shall examine the precise flow profile for a complex food material contained within the gap of a cone-and-plate rheometer just so as to test that assumption. In particular, we shall be concerned to examine that assumption where yield stress characteristics are present.

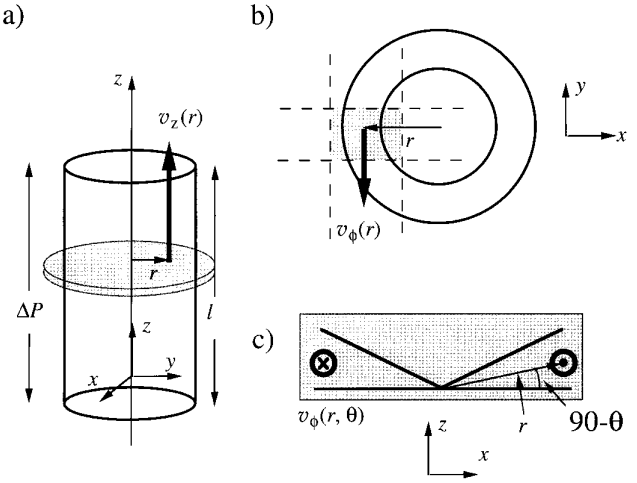

Figure 3. Geometry relevant to flow imaging in (a) pipe, (b) cylindrical Couette cell and (c) cone-and-plate rheometer. The shaded areas show the image planes used in this work while the Cartesian axes correspond to the gradient orientations for the respective pulse sequences shown in Fig. 4.

In the remaining geometries of interest, the pipe and cylindrical Couette cell, the fluid is not subjected to uniform stress but, instead, the stress varies across the gap in a well defined manner. (We shall assume throughout this paper that the velocities are sufficiently small that inertial effects may be neglected, which is certainly the case for flow in most food materials where the Reynolds number, *Re*, is normally small.) For such a flow a wide section of the flow curve is participating at any given flow rate. This suggests that a measurement of the velocity profile should provide flow curve information directly.[12] The two flow configurations are shown in Fig. 3(a) and (b). In the pipe the stress varies uniformly with radius and has zero value at the pipe centre. In the cylindrical Couette cell the stress is inversely proportional to radius squared, thus exhibiting a maximum at the inner wall and a minimum (but non-zero) value at the outer surface. In the limit of very small gap the stress can be made approximately uniform.

We shall be concerned with NMR velocimetry in the pipe and cylindrical Couette arrangements for two reasons. First, we shall be able to use these as simple devices for the measurement of flow curve properties and, especially, we shall be able to elucidate bulk flow curve characteristics without the ambiguous influence of apparent slip, should such effects be present. Second, we shall be concerned with looking at the details of flow behaviour. For example, in the case of pipe flow, we may seek to characterize apparent slip behaviour, whereas in the case of the cylindrical Couette cell, we observe the details of flow when yield stress plays a role in determining the fluid response.

In a cylindrical pipe, the shear rate is related to the velocity profile, $v_z(r)$, by

$$\dot{\gamma} = \frac{\partial v_z}{\partial r} \tag{1}$$

Consider a cylinder of fluid of radius r and length l sited in the flow such that the pressure drop along the length

© 1997 John Wiley & Sons, Ltd.

of the cylinder is ΔP. The shear stress exerted on the cylinder surface is simply

$$\sigma = (\Delta P/2l)r \tag{2}$$

The linear dependence of stress, σ, on radical displacement, r, is a particularly useful result since it enables one to derive the flow curve directly from the tube velocity profile by calculating the derivative, $\partial v_z/\partial r$. If the parameter $\Delta P/2l$ has been measured in the experiment, then this curve will be absolute in both σ and $\dot{\gamma}$.

The simple relationship which exists between the velocity profile in a pipe and the flow curve leads to analytical expressions for the velocity when the σ *vs.* $\dot{\gamma}$ equation is also analytical. One simple example is the power law fluid constitutive equation ($\sigma = m\dot{\gamma}^n$) for which the fluid will be shear-thinning when $n < 1$ and shear-thickening when $n > 1$. The radical dependence of velocity in the pipe is represented by[13]

$$v_z(r) = v_{max}[1 - (r/a)^{(n+1)/n}] \tag{3}$$

where a is the pipe radius. While this relationship will not be particularly useful in characterizing a fluid exhibiting rheological discontinuities, it does represent a reference against which deviations can be ascertained.

For cylindrical Couette flow, the relationship between the shear rate and the azimuthal velocity profile, $v_\phi(r)$, is given by

$$\dot{\gamma} = \frac{\partial v_\phi}{\partial r} - \frac{v_\phi}{r} \tag{4}$$

The equation of motion for a power-law fluid in steady cylindrical Couette flow may also be solved to obtain an analytical expression for v_ϕ at radius r. In the case of a stationary outer cylinder of inside radius r_o and an inner cylinder of outside radius r_i rotating at angular speed Ω, the velocity is given by[14]

$$v_\phi = \Omega r_i \frac{R(1 - R^{-2/n})}{K(1 - K^{-2/n})} \tag{5}$$

where $K = r_i/r_o$ and $R = r/r_o$. Using Eqn (4), the corresponding expression for the shear rate is

$$\dot{\gamma} = \frac{2\Omega}{n} \frac{R^{-2/n}}{1 - K^{-2/n}} \tag{6}$$

NMR MICROSCOPY AND VELOCITY IMAGING

A detailed description of NMR microscopy and velocity imaging can be found elsewhere[15] and only the basic principles will be given here. The method depends on the imposition of a magnetic field gradient. $\mathbf{G} = \mathbf{grad}B_0$, a vector which describes components of the gradient in the main polarizing field, B_0. Hence we write the local spin precession frequency as

$$\omega(r) = \gamma B_0 + \gamma \mathbf{G} \cdot \mathbf{r} \tag{7}$$

This simple linear relationship between the Larmor frequency and the nuclear spin coordinates, **r**, encapsulates the imaging principle.[16] Since each isochromat of spins at position **r** precesses at local offset frequency $\gamma \mathbf{G} \cdot \mathbf{r}$, the net signal in the heterodyne detection frame may be written as[15,16]

$$S(\mathbf{k}) = \int \rho(\mathbf{r}) \exp(i2\pi \mathbf{k} \cdot \mathbf{r})\, d\mathbf{r} \tag{8}$$

where $\rho(\mathbf{r})$ is the nuclear spin density and **k** is the reciprocal space dimension conjugate to **r** and given by $(1/2\pi)\gamma \mathbf{G}t$, t being the evolution time. The nuclear spin density can be reconstructed by acquiring $S(\mathbf{k})$ over some appropriate volume of **k** space and performing an inverse Fourier transformation, generally in two dimensions using a plane of spins prepared by a frequency-selective excitation. The high spatial resolution needed for NMR microscopy[15] depends on the use of a large polarizing field ($\gtrsim 5$ T), small receiver coils of high sensitivity and gradient coils capable of delivering in excess of 20 G cm^{-1}.

In order to image velocity we further encode the signal with a pulsed gradient spin echo (PGSE) pair,[15,17] as shown in the pulse sequence in Fig. 4. These pulses define a second wave vector domain, **q**, and impart a phase shift to the spin isochromat which depends directly on the motion of those spins. In particular, a spin moving by $\mathbf{R} = \mathbf{r}' - \mathbf{r}$ over the time Δ between the PGSE pulse pair acquires a phase factor

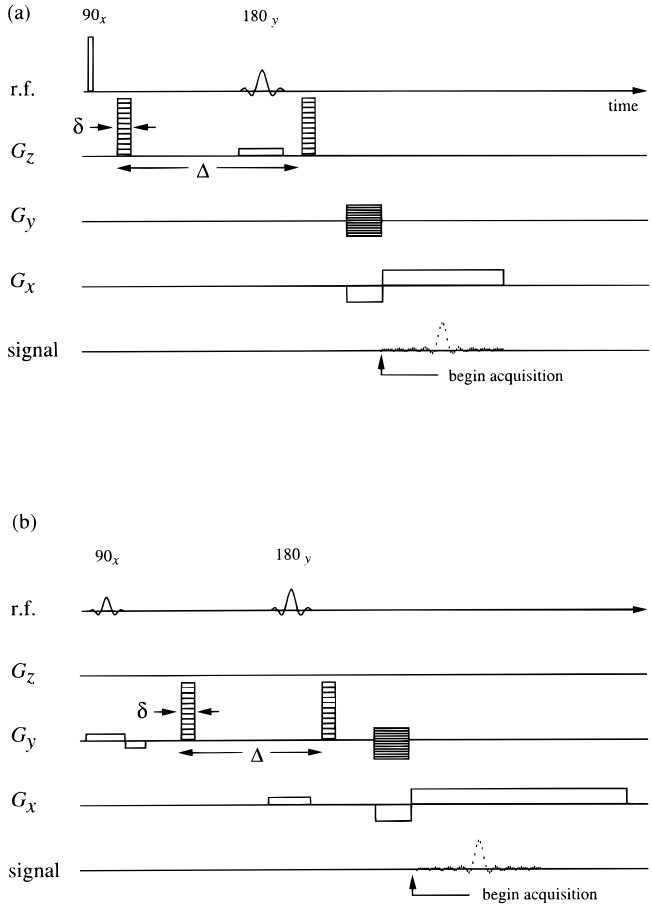

Figure 4. R.f. and gradient pulse sequences used to image velocity. (a) Velocity-encoding PGSE pulses normal to the slice (i.e. along the z-direction); this is the sequence used for the pipe and cone-and-plate experiments. (b) Two orthogonal slice selection gradients are used to excite the shaded region for the Couette cell shown in Fig. 3(b). The velocity-encoding PGSE pulses are oriented along the phase-encoding direction (i.e. y-axis).

© 1997 John Wiley & Sons, Ltd.

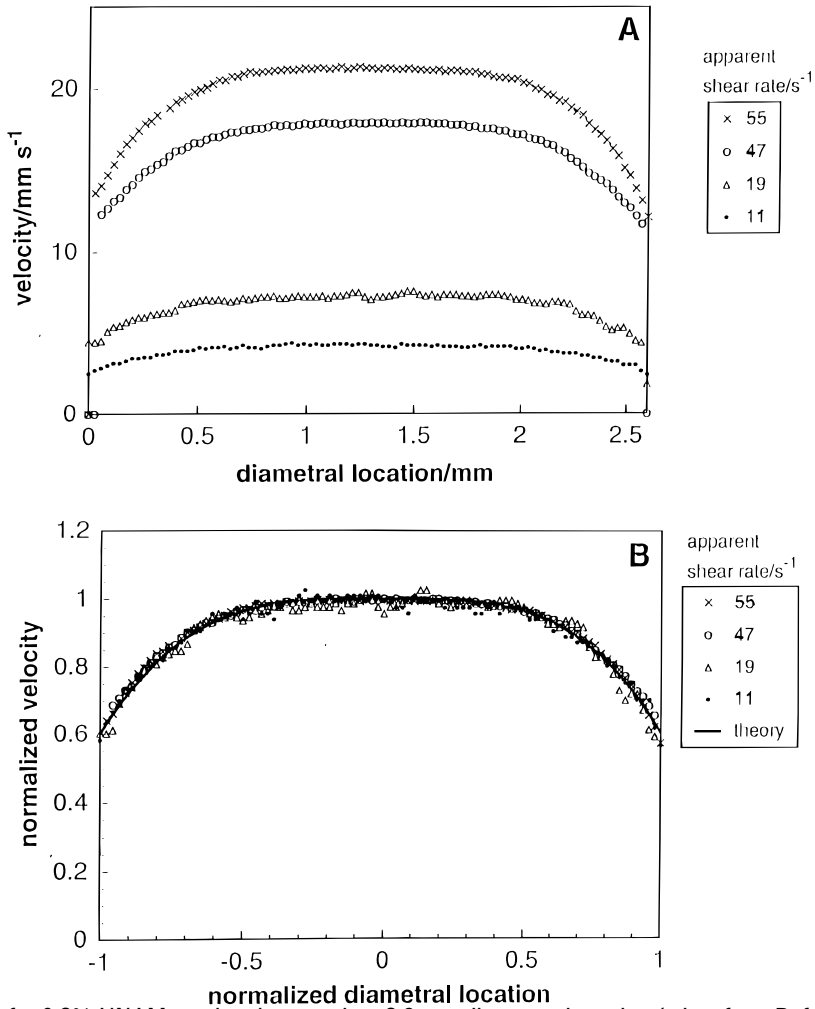

Figure 5. Velocity profiles for 0.2% UNAM xanthan in water in a 2.6 mm diameter glass pipe (taken from Rofe *et al.*[20] and reproduced by permission from the *Journal of Rheology*). (A) Absolute velocity profiles; (B) normalized plot and theoretical curve [Eqn (3)] for slip 60% of the maximum velocity and power law index $n = 0.39$.

$\exp(i2\pi\mathbf{q}\cdot\mathbf{R})$. This constrast factor means that the signal acquired is effectively modulated both in **k**- and **q**-space.[15,18] Thus,

$$S(\mathbf{k}, \mathbf{q}) = \int \rho(\mathbf{r}) \left[\int \overline{P}_s(\mathbf{R}, \Delta) \exp(i2\pi\mathbf{q}\cdot\mathbf{R})\, d\mathbf{R} \right] \times \exp(i2\pi\mathbf{k}\cdot\mathbf{r})\, d\mathbf{r} \quad (9)$$

where, implicitly, $\overline{P}_s(\mathbf{R}, \Delta)$ is the average propagator at each pixel **r** of the image and describes the probability distribution of displacements **R** for all spins in that pixel. Double inverse Fourier transformation of $S(\mathbf{k}, \mathbf{q})$ with respect to both **k** and **q** gives $\rho(\mathbf{r})\overline{P}_s(\mathbf{R}, \Delta)$. By normalizing this function with the image density $\rho(\mathbf{r})$ acquired under zero PGSE gradient, one reconstructs $P_s(\mathbf{R}, \Delta)$ for each pixel of the image.

We conventionally apply the **q** gradient in a single direction in any given experiment, and define the component of **R** along **q** as Z. The magnitude $q = |\mathbf{q}|$ is stepped in value from zero to some maximum number, n_D, of order 10. Thus a series of images is obtained at different q values and the modulated image signal in each pixel is Fourier transformed along the q-direction to give $\overline{P}_s(Z, \Delta)$ for that pixel.[19] The method is time consuming, taking of the order or 30 min to acquire a velocity image, but given that this time is also used to enhance the signal-to-noise ratios, an important issue in NMR microscopy, it is well spent.

Our image analysis software automatically processes these average propagators, using the width of $\overline{P}_s(Z, \Delta)$ to estimate the r.m.s. Brownian motion $(2D_s\Delta)^{1/2}$ and the displacement of $\overline{P}_s(Z, \Delta)$ along the Z-axis to estimate the flow displacement $v\Delta$. In this manner, maps of $D_s(\mathbf{r})$ and $v(\mathbf{r})$ may be constructed. Although the method depends on steady-state flow conditions in the sample, it does have the advantage of returning accurate and precise velocity maps. The sensitivity of the method is very high, permitting velocity resolution of the order of 10 μm s^{-1}.

EXPERIMENTAL

Pipe flow in a xanthan gum solution

Our first example concerns the pipe flow of a solution of xanthan gum, work reported by Rofe *et al.*[20] They pumped a 0.2% solution of xanthan in distilled water through a variety of glass pipes of different diameters. Xanthan gum solutions provide an example of a shear-thinning fluid which can exhibit significant apparent slip. In the study of Rofe *et al.*, the degree of slip was

© 1997 John Wiley & Sons, Ltd.

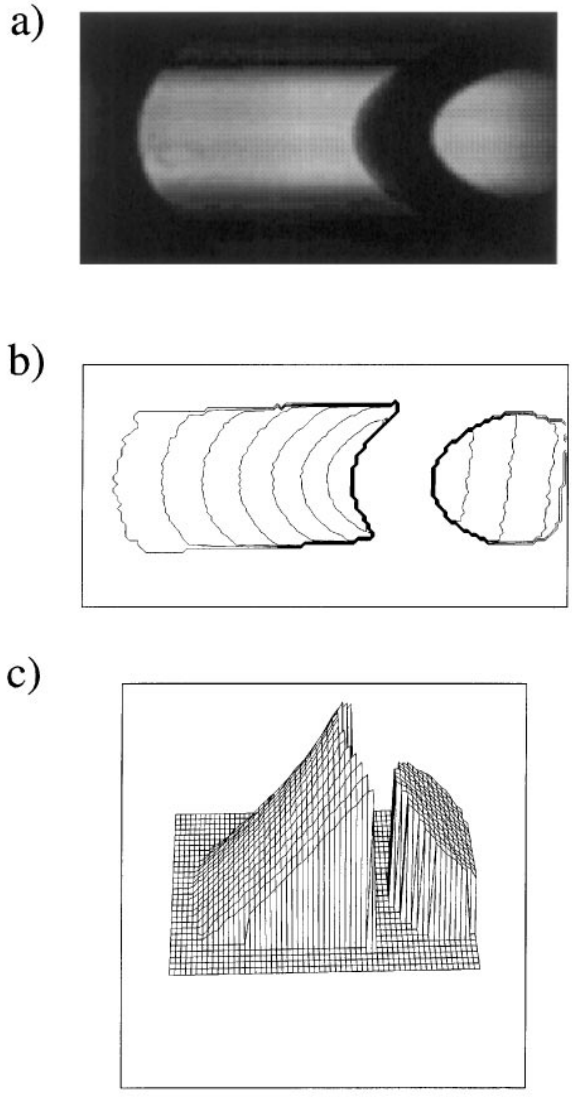

Figure 6. (a) Image of water in the cylindrical Couette cell. The slice selection sequence in Fig. 4(b) is used to produce a signal only in the chosen region incorporating the annulus and part of the central (marker fluid) space. The horizontal field of view is 4.5 mm while the resolution in the vertical direction is smaller by a factor of 0.45, giving pixel dimensions of 35 × 78 μm; hence the elliptical appearance of the cylinders. The small delay between phase and read-encoding results in a slight rotation of the image. Velocity profiles for Figs 7–10 are selected across the central horizontal diameter line. (b) Contour plot of the water velocity map and (c) stacked profile plot of the water velocity map.

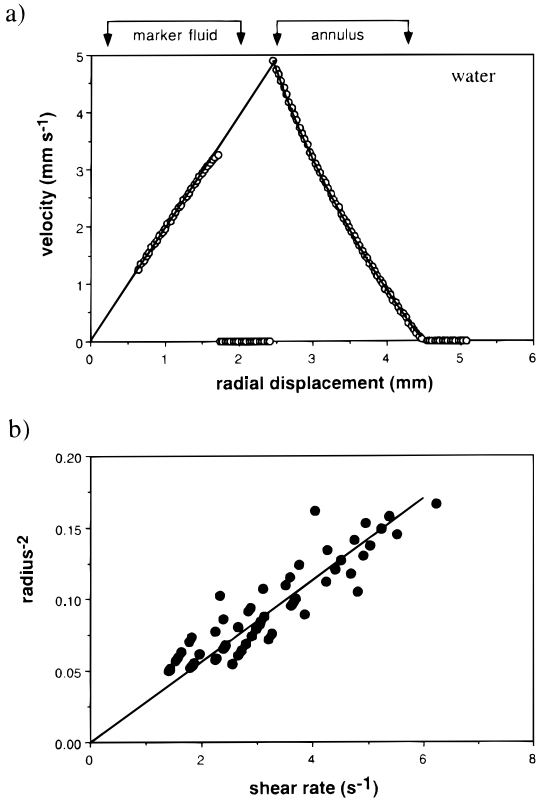

Figure 7. (a) Radial velocity profile taken across the cylindrical Couette cell for the case of water. The fit in the annular region is obtained using Eqn (5) and with $n = 1$. (b) Flow curve calculated from the data shown in (a). The shear rate using is obtained Eqn (4).

shown to depend on the source of xanthan and to correlate with polymer molecular weight. In those experiments, the xanthan used was obtained from UNAM (Mexico City, Mexico).

A sample velocity profile from the work of Rofe *et al.*[20] is reproduced in Fig. 5(a) Details of the experimental parameters can be found in the original paper. Apparent slip is evident. Figure 5(b) shows velocity profiles at different pump flow rates which have been normalized on the maximum velocity in each case. Universal behaviour is evident and the data have been overlaid with a theoretical profile that was calculated by estimating the normalized slip velocity (as 0.6) from the maximum velocity in the pixel adjacent to the wall and adding that to the appropriately normalized predicted power law profile (Eqn (3)]. The power law index is found to be 0.39, consistent with strong shear-thinning behaviour. It also agrees closely with the index obtained by direct measurement of viscosity *vs.* shear rate using a standard cone-and-plate rheometer. Rofe *et al.* measured a wide range of absolute slip velocities and showed that they depended uniquely on wall stress. In this work, the NMR measurements of apparent slip agreed well with indirect measurements using the Mooney method[21] of analysis of pipe flow rates.

Cylindrical Couette flow in a variety of food materials

Just as the pipe forms a useful geometry for investigating a segment of the flow curve covering a range of stress and shear rates, so the cylindrical Couette cell, with its simple dependence of stress on radial position, can serve the same function. However, the Couette cell has the distinct advantage that it contains a fixed amount of fluid within the annulus between the cylinders rather than requiring a reservoir of fluid to be pumped through. It is therefore well suited to rheological studies on small samples. Our rheometer consists of two concentric glass tubes with outer tube of inner diameter 9 mm and inner tube of outer diameter 5 mm, located inside the 15 mm resonator of the microimaging probehead. The inner tube is rotated by a long shaft which passes down the bore of the 7 T magnet from a stepping motor/gearbox controller.

We shall demonstrate here the use of this particular device to investigate the shear-dependent viscosity of a

© 1997 John Wiley & Sons, Ltd.

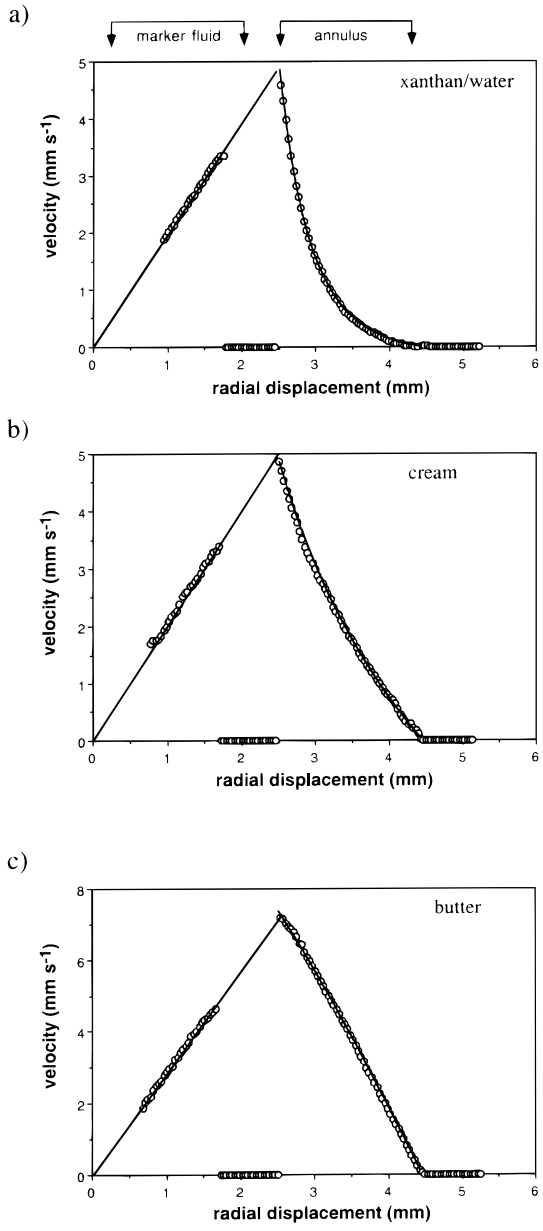

Figure 8. Radial velocity profiles taken across the cylindrical Couette cell for three cases. (a) Sigma xanthan in water at 25 °C. The fit in the annular region is using Eqn (5) and with $n = 0.28$. (b) Cream at 25 °C. The fit using Eqn (5) yields $n = 0.8$. (c) Semi-soft butter at 40 °C. The fit using Eqn (5) yields $n = 3.0$.

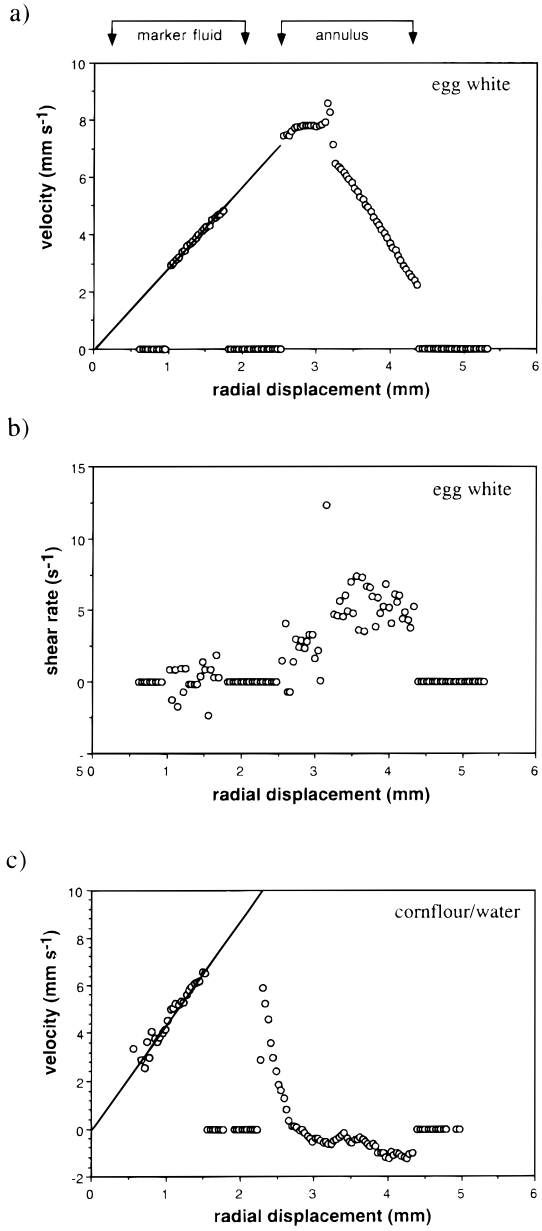

Figure 9. (a) Radial velocity profile taken across the cylindrical Couette cell for egg white at 25 °C. A separation of different shearing bands is apparent within the annulus. (b) Corresponding shear rate *vs*. radius for the data in (a). The shear rate is obtained using Eqn (4). (c) Radial velocity profile taken across the cylindrical Couette cell for cornflour–water mixture at 25 °C.

wide range of food materials. We begin, however, with a Newtonian water reference in which the central cylinder is rotated at 0.31 Hz. Figure 6(a) shows a 128 × 128 pixel image of the selected annular region in the water-filled Couette cell, in accordance with the schematic diagram shown in Fig. 3(b). The central tube is also filled with water to provide a marker. The field of view is 4.5 mm in the x-direction and 10 mm in the y-direction, so that the circular cross-section appears elliptical. Using the pulse sequence in Fig. 4(b), a velocity image was obtained at 25 °C using eight q-slices with $\delta = 2.5$ ms, $\Delta = 30$ ms and with a maximum q-gradient of 18 G cm^{-1} (two acquisitions were used with a repetition time of 1 s). We display these image data as velocity contour and perspective stacked profile plots in Fig. 6(b) and (c).

A profile across the centre of the velocity image is shown in Fig. 7. The unsheared marker fluid in the central tube provides a useful reference and, by extrapolation, the velocity of the inner tube surface can be found in order to test the non-slip boundary condition. The velocity profile in the gap was fitted using the power law relationship in Eqn (5) and yields the required exponent $n = 1$.

In principle, the data can be analysed by obtaining the shear rate directly using Eqn (4), and then calculating a flow curve using the fact that the shear stress varies as r^{-2}. The results are shown in Fig. 7(b). Because the differentiation process introduces significant noise into the data, we prefer to fit the velocity

© 1997 John Wiley & Sons, Ltd.

profile data directly in order to obtain information about the shear dependence of viscosity.

We used the Couette cell system to investigate the non-linear viscosity of a variety of food products, including the food thickener xanthan gum (Sigma Chemicals, St Louis, MO, USA) in water, cream (Tararua, Pahiatua, New Zealand), semi-soft butter (Anchor Fernleaf, Takanini, Auckland New Zealand), egg-white (hen egg), cornflour–water, mixture (Ritz, Auckland, New Zealand) and two varieties of tomato sauce (Heinz, Dandenong, Victoria, Australia and Whitlock's, East Tamaki, Auckland, New Zealand). All experiments were performed at 25 °C with the exception of those for the semi-soft butter, which was sheared at 40 °C.

The results from each of the food products are remarkably different. Figure 8 shows the profiles for xanthan gum (0.2% w/v in distilled water), for cream and for semi-soft butter. The inner cylinder rotation speeds were 0.31, 0.31 and 0.47 Hz, respectively. In each case a no-slip boundary condition is observed at both the inner and outer walls and the velocity profile varies smoothly with radius, akin to the behaviour of a power law fluid. However, the dependence of shear rate on radius and the fitted power law exponents differ greatly between the fluids. The Sigma xanthan gum solution is strongly shear-thinning ($n = 0.28$), this power law exponent being significantly lower than that exhibited by the UNAM xanthan. The cream is also shear-thinning, although weakly so ($n = 0.8$). By contrast, the butter shows shear-thickening behaviour with $n = 3$. We cannot resist a remark, *en passant*, that the rheology of semi-soft butter is of some interest, given the controversy surrounding the entry of this new food into the European market, and especially give the commercial significance of this product to the New Zealand economy.

While each of the examples shown in Fig. 8 exhibits single-phase properties across the shearing annulus, a dramatically different behaviour is found in the cases of egg white, cornflour in water (80% by volume) and tomato sauce. The inner cylinder rotations speeds were 0.47, 0.63 and 0.85 Hz, respectively. The profiles for egg white and cornflour in water are shown in Fig. 9. The egg white exhibits a remarkable change in shear rate with a low shear region close to the inner cylinder (high-stress region) and a high shear rate in the outer region of the annulus. A sharp transition is apparent with some instability evident at the interface. The data are plotted as shear rate *vs.* radius in Fig. 9(b), where Eqn (4) has been used to obtain the local shear rates directly from the velocity profile. We attribute this heterogeneity to a shear-induced phase transition in the egg white in the high-stress region. We further note that in the high-stress region there is no slip at the inner shearing surface while slip clearly exists at the outer shearing surface.

The cornflour–water data are shown in Fig. 9(c). Again, a dramatic phase transition is apparent within the annulus. However, with this material the higher stress region exhibits high shear while the outer annulus is plug-like with velocity very close to zero, and actually negative near the outer wall. This latter behaviour is extraordinary and we attribute it to a backflow of water as the plug is dragged around. The shear-thickening properties of cornflour–water mixtures are well known and can be graphically demonstrated in a simple stirring test. What is remarkable about the present experiment is that the thickening process occurs at some distance from the point of shear stress application, as indicated by the inflection in the velocity profile. This intriguing property can also be seen in the stirring test. Indeed, we would argue that it is akin to a process well known in another shear-thickening particulate material, sand and water. Application of pressure to wet sand results in a squeezing out of water, and consequent thickening, away from the source of pressure while repeated local stress results in a wetting/softening process.

Finally, we show in Fig. 10 a comparison of the shear-dependent viscous properties of the two different brands of tomato sauce. The Heinz sauce in Fig. 10(a) exhibits shear-thinning behaviour right across the gap but with significant slip at both the inner and outer shearing surfaces. Furthermore, there is a transition in the behaviour of the fluid at mid-annulus with the rate of shear changing discontinuously. In the inner (high-stress) band the velocity gradient is similar to that expected for a Newtonian fluid. In the outer band the velocity gradient exhibits strong curvature, indicative of shear-thinning. The Whitlock's sauce has an even higher slip at the inner surface and also exhibits a variable shear across the annulus, finally exhibiting low slip at the outer surface. However, the shear rate behaviour

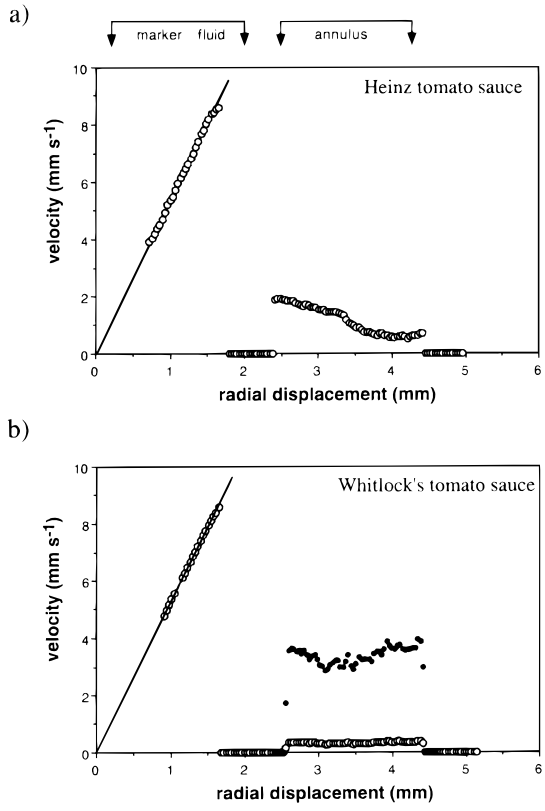

Figure 10. (a) Radial velocity profiles taken across the cylindrical Couette cell for (a) Heinz tomato sauce and (b) Whitlock's tomato sauce, both at 25 °C. Both fluids exhibit slip and shear banded flow but the Whitlock's sauce manifests yield stress behaviour. The closed circles show the velocity within the gap at 10 × gain.

© 1997 John Wiley & Sons, Ltd.

across the annulus is significantly different for this variety of tomato sauce. Once again a transition in shear rate is observed within the annulus, the velocity first decreasing and then increasing with radius in a manner akin to plug flow but the inner (high stress) band is shear-thinning whereas the outer is plug-like. The separation into separate shear thinning and plug-like phases represents a behaviour characteristic of yield stress properties, a feature which corresponds well with the observed macroscopic properties of this brand of sauce.

Cone-and-plate flow

We have recently developed a series of cone-and-plate rheometers which fit inside the 25 mm resonator of the micro-imaging probehead and driven by the same rotation shaft as described earlier. The cone-and-plate surfaces are made from the machinable glass product, Macor (Corning, New York, USA) and the cone angle is 7°. Figure 11(a) shows an image of water within the gap. The horizontal field of view is 25 mm with a slice thickness of 2 mm. By using a larger gradient in the z-direction the scale is expanded along this axis by a factor of three, thus making the gap angle appear significantly larger. Velocity encoding was carried out using eight q-steps with $\delta = 2$ ms, $\Delta = 15$ ms, maximum gradient 18 G cm^{-1}, four acquisitions and a repetition time of 1 s. Velocity imaging experiments were carried out for water (rotation speed 0.13 Hz) and Whitlock's tomato sauce (0.27 Hz). In order to illustrate the velocity distribution within the gap we display the velocity maps in Figs 11 and 12 both as contour plots and as a stacked-profile plot in perspective view. The water, as expected, exhibits a uniform shear rate in the gap without slip. The Whitlock's tomato sauce clearly slips predominantly at the lower plate, again in the region of maximum stress as we have remarked in the Couette experiment, although we note that the stress difference across the surfaces is much smaller, around 1.5% for the cone-and-plate compared with 250% in the Couette cell.

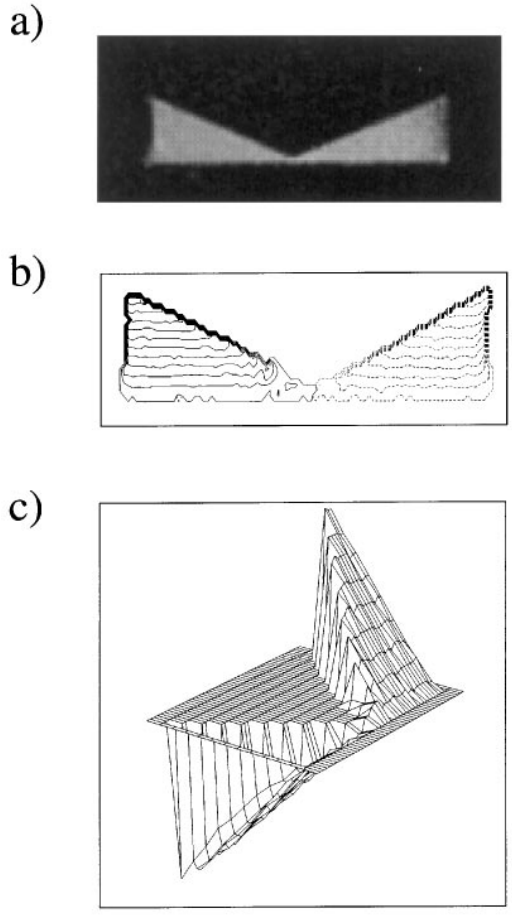

Figure 11. (a) Image of water in the cone-and-plate cell corresponding to the schematic diagram in Fig. 3(c). The horizontal field of view is 25 mm while the resolution in the vertical direction is larger by a factor of three, giving pixel dimensions of 195 × 65 μm. (b) Contour plot of the water velocity map and (c) stacked profile plot of the water velocity map. The water exhibits the expected constant shear rate and no slip at the boundary.

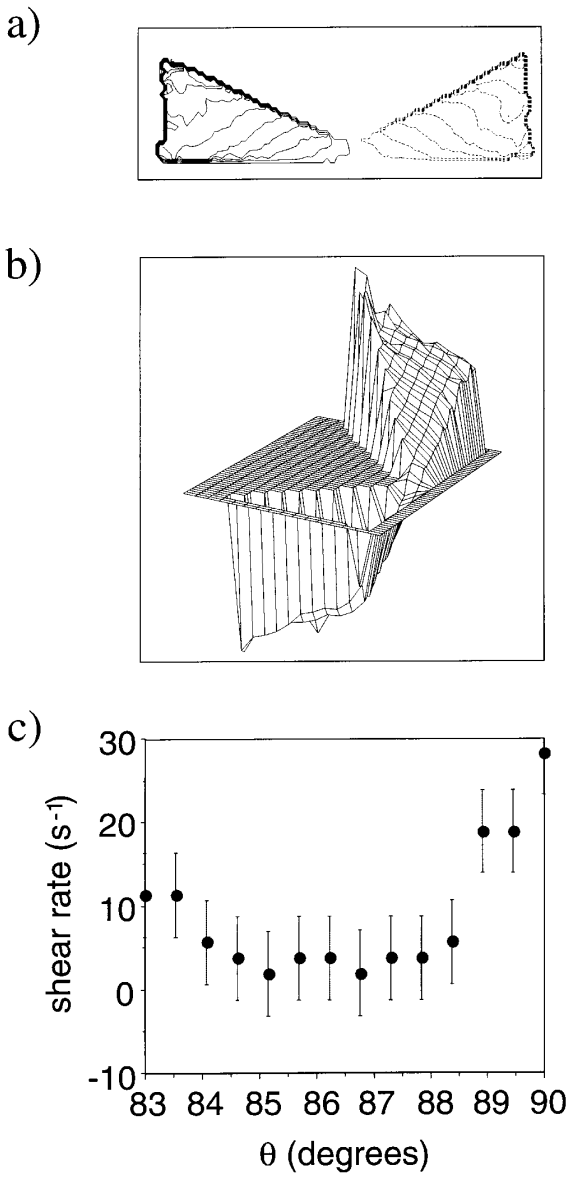

Figure 12. Velocity maps and shear rate for Whitlock's tomato sauce in the cone-and-plate cell. (a) Contour plot of the fluid velocity map and (b) stacked profile plot of the fluid velocity map. The tomato sauce exhibits slip and a non-uniform rate of strain across the gap. (c) Derivative along a vertical velocity profile showing the shear rate and apparent banding structure.

© 1997 John Wiley & Sons, Ltd.

Furthermore, we again find evidence for a non-uniform rate of strain within the bulk of the fluid, despite the highly uniform stress which exists across the gap in the cone-and-plate device. To emphasize this point we show the gap shear rate profile in Fig. 12(c). In this case the low shear rate plug region is centred within the gap and is bounded by two shearing phases.

Non-uniformity of rate of strain within the gap of a cone-and-plate rheometer runs counter to the assumptions which underpin the use of this device. We suggest that this property must arise from discontinuity in the flow curve for the sauce, indicative of complex constitutive behaviour associated with yield stress.

CONCLUSIONS

The experiments reported here demonstrate the utility of NMR velocity profiling experiments in the study of non-linear flow properties in food materials. We note that the use of microscopic resolution has allowed the investigation of small samples at relatively high shear rates. However, more than that, they show that such NMR measurements profile a vital adjunct to any conventional rheometric study. The food products investigated in this work have variously exhibited shear-thinning, shear-thickening, apparent slip, stress-related phase separation and shear rate heterogeneity. Because of the prevalence of these diverse pathologies in food samples under shear, any assumptions based on external stress and strain-rate measurements alone may well be in serious error. We would argue that it is essential to investigate shear rate with some spatial resolution if rheometric measurements on these materials are to be properly understood.

There is another sense in which the NMR measurements have significance. In this paper we have demonstrated that we may spatially resolve differing regions of material in which the local viscosity differs markedly. Given that resolution, it becomes possible, in principle, to apply NMR spectroscopic techniques in order to understand the molecular basis of the mechanical behaviour. In particular, one might measure molecular diffusion coefficients, spin relaxation times and molecular order parameters via higher spin–spin interactions, and to do so with spatial resolution in each of the identified phases. The combination of such spectroscopic techniques with velocity imaging could become a powerful tool for rheo-NMR investigations of molecular interactions in complex fluids.

Acknowledgements

We gratefully acknowledge funding support from the New Zealand Foundation for Research, Science and Technology.

REFERENCES

1. K. Walters and N. D. Waters, *Polymer Systems: Deformation and Flow*. Macmillan, London (1968).
2. K. Walters, *Rheometry*. Chapman and Hall, London (1975).
3. R. W. Whorlow, *Rheological Techniques*. Ellis Horwood, New York (1992).
4. H. A. Barnes, J. J. Hutton and K. Walters, *An Introduction to Rheology*. Elsevier, Amsterdam (1989).
5. M. Doi and S. F. Edwards, *The Theory of Polymer Dynamics*. Oxford University Press, Oxford (1987).
6. T. C. B. McLeish and R. C. Ball, *J. Polym. Sci.* **24**, 1735 (1986).
7. M. E. Cates, T. C. B. McLeish and G. Marrucci, *Europhys. Lett.* **21**, 451 (1993).
8. N. A. Spenley, X. F. Yuan and M. E. Cates, *J. Phys. II* (*Paris*) **6**, 551 (1996).
9. H. Rehage and H. Hoffman, *J. Phys. Chem.* **92**, 4712 (1988).
10. M. E. Cates, *Macromolecules* **20**, 2289 (1987).
11. M. E. Cates, *J. Phys. Chem.* **94**, 371 (1990).
12. P. T. Callaghan, M. E. Cates, C. J. Rofe and J. B. A. F. Smeulders, *J. Phys. II* (*Paris*) **6**, 375 (1996).
13. A. H. P. Skelland, *Newtonian Flow and Heat Transfer*. Wiley, New York (1967).
14. C. J. Rofe, R. K. Lambert and P. T. Callaghan, *J. Rheol.* **38**, 857 (1994).
15. P. T. Callaghan, *Principles of Nuclear Magnetic Resonance Microscopy*. Oxford University Press, Oxford (1991).
16. P. Mansfield and P. G. Morris, *NMR Imaging in Biomedicine*. Academic Press, New York (1982).
17. E. O. Stejskal and J. E. Tanner, *J. Chem. Phys.* **42**, 288 (1965).
18. P. T. Callaghan, C. D. Eccles and Y. Xia, *J. Phys. E* **21**, 820 (1988).
19. P. T. Callaghan and Y. Xia, *J. Magn. Reson.* **91**, 326 (1991).
20. C. J. Rofe, L. de Vargas, J. Pérez-González, R. K. Lambert and P. T. Callaghan, *J. Rheol.* **40** 1115 (1996).
21. M. Mooney, *J. Rheol.* **2**, 210 (1931).

© 1997 John Wiley & Sons, Ltd.